



HAL
open science

Identification of phosphorus sites in amorphous LiPON thin film by observing internuclear proximities

Racha Bayzou, Julien Trébos, Annie-Kim Landry, Rafael Nuernberg, Brigitte Pecquenard, Frédéric Le Cras, Frédérique Pourpoint, Olivier Lafon

► To cite this version:

Racha Bayzou, Julien Trébos, Annie-Kim Landry, Rafael Nuernberg, Brigitte Pecquenard, et al.. Identification of phosphorus sites in amorphous LiPON thin film by observing internuclear proximities. Journal of Magnetic Resonance, 2023, 354, pp.107530. 10.1016/j.jmr.2023.107530 . hal-04193774

HAL Id: hal-04193774

<https://hal.science/hal-04193774>

Submitted on 16 Oct 2023

HAL is a multi-disciplinary open access archive for the deposit and dissemination of scientific research documents, whether they are published or not. The documents may come from teaching and research institutions in France or abroad, or from public or private research centers.

L'archive ouverte pluridisciplinaire **HAL**, est destinée au dépôt et à la diffusion de documents scientifiques de niveau recherche, publiés ou non, émanant des établissements d'enseignement et de recherche français ou étrangers, des laboratoires publics ou privés.

Identification of phosphorus sites in amorphous LiPON thin film by observing internuclear proximities

Racha Bayzou^a, Julien Trébosc^b, Annie-Kim Landry^{c,d}, Rafael B. Nuernberg^c,
Brigitte Pecquenard-Le Cras^c, Frédéric Le Cras^d, Frédérique Pourpoint^a, Olivier Lafon^{a,*}

^a Univ. Lille, CNRS, Centrale Lille, Univ. Artois, UMR 8181 – UCCS – Unité de Catalyse et Chimie du Solide, 59000 Lille, France

^b Univ. Lille, CNRS, INRAE, Centrale Lille, Univ. Artois, FR 2638 – IMEC – Fédération Chevreul, 59000 Lille, France

^c Univ. Bordeaux, CNRS, Bordeaux INP, ICMCB, UMR 5026, 33600 Pessac, France

^d Univ. Grenoble Alpes, CEA, LITEN, DEHT, 38000 Grenoble, France

ABSTRACT

Keywords:

LiPON

Thin films

solid-state NMR

³¹P NMR

³¹P-¹⁴N proximities

³¹P-³¹P proximities

Amorphous lithium phosphorus oxynitrides (LiPON), prepared by reactive magnetron sputtering, have become the electrolytes of choice for all-solid-state thin film microbatteries since its discovery in early 1990s. Nevertheless, there is still a lack of understanding of their atomic-level structure and its influence on ionic conductivity. Solid-state NMR spectroscopy represents a promising technique to determine the atomic-level structure of LiPON glasses but is challenging owing to its low sensitivity in the case of thin film materials. Recently, ³¹P solid-state NMR spectra of LiPON thin films were acquired under magic-angle spinning (MAS) conditions and assigned with the help of density functional theory (DFT) calculations of NMR parameters. However, the identification of the different P local environments in these materials is still a challenge owing to their amorphous structure and the lack of resolution of the ³¹P MAS NMR spectra. We show herein how the NMR observation of internuclear proximities helps to establish the nature of P sites in LiPON thin films. The ³¹P-¹⁴N proximities are probed by a transfer of population in double resonance (TRAPDOR) experiment, whereas ³¹P-³¹P proximities are observed using one-dimensional (1D) ³¹P double-quantum (DQ)-filtered and two-dimensional (2D) ³¹P homonuclear correlation spectra as well as dipolar dephasing experiments using DQ-DRENAR (DQ-based dipolar-recoupling effects nuclear alignment reduction) technique. The obtained NMR data further support the recently proposed assignment of ³¹P NMR signals of LiPON thin films. With the help of this assignment, the simulation of the quantitative 1D ³¹P NMR spectrum indicates that PO₄³⁻ orthophosphate anions prevail in LiPON thin films and N atoms are mainly incorporated in [O₃PNPO₃]⁵⁻ dimeric anions. PO₃N⁴⁻ isolated tetrahedra and [O₃POPO₃]⁴⁻ anions are also present but in smaller amounts.

1. Introduction

With the development of microelectronics and the internet of things, there is an increasing demand for embedded power sources for autonomous microsystems, such as implantable biosensors, microactuators and other microelectromechanical systems (MEMS) [1,2]. In this regard, all-solid-state lithium microbatteries offer the advantage of high energy density and high level of possible miniaturization. The solid electrolyte is a key element of microbatteries in that it conditions both the performance and the manufacturing process of these devices. Amorphous lithium phosphorus oxynitride, LiPON, pioneered at Oak Ridge National Laboratory [3], is used as thin film electrolyte in most commercial all-

solid-state lithium microbatteries since it combines fairly good ionic conductivity (2–3 μS.cm⁻¹) at room temperature, low electronic conductivity (<0.1 pS.cm⁻¹), and a suitable electrochemical stability against Li metal anodes and high-energy density cathode materials. Furthermore, the combination of its suitable mechanical properties, its low electronic conductivity and the absence of grain boundaries in these thin films prevents the formation of dendrites and results in a remarkable cycle life. LiPON thin films with a typical thickness of 1 μm are usually prepared by radiofrequency (rf) reactive sputtering of Li₃PO₄ target in N₂ plasma [4–6].

Nevertheless, their atomic-level structure and the relationships between their structure and the ionic conductivity are still under debate.

* Corresponding author.

E-mail address: olivier.lafon@univ-lille.fr (O. Lafon).

The major questions raised are related to the type of structural units and the nature of nitrogen sites [7,8]. Initially, N1s X-ray photoelectron spectra (XPS) suggested the presence of nitrogen atoms bound to two and three P atoms [3–6]. These doubly and triply coordinated nitrogen atoms are denoted N_d and N_t , respectively. Recently, ab initio molecular dynamics (AIMD) simulations, combined with neutron scattering, confirmed the presence of N_d sites but pointed to the presence of apical nitrogen (N_a) atoms bound to a single P, instead of N_t [8,9].

This structural model was applied to interpret the one-dimensional (1D) ^{31}P NMR spectrum of LiPON thin films prepared by rf sputtering under magic-angle spinning (MAS) conditions [10]. This study by Marple *et al.* was the first to report NMR data for LiPON thin films prepared by rf sputtering, which is the actual material present in microbatteries. Previous NMR spectra of LiPON reported in the literature were only acquired for bulk glasses, which contain smaller molar fraction of Li element [11] or thin films deposited by ion-beam assisted deposition (IBAD) [12]. In fact, the lack of sensitivity of solid-state NMR spectroscopy is a limitation for the study of amorphous and volume-limited samples, such as LiPON thin films. Another difficulty is that LiPON thin films are air-sensitive and the NMR samples must be prepared in inert atmosphere.

Furthermore, the NMR spectra of LiPON thin films are challenging to assign since these amorphous materials contain a distribution of local environments, which results in broad overlapping NMR resonances. Tentative deconvolution and assignment of ^{31}P NMR signals of LiPON thin films prepared by rf sputtering were proposed with the help of DFT calculations of ^{31}P isotropic chemical shifts (δ_{iso}) and chemical shift anisotropy (CSA) for a wide range of phosphorus-containing crystals as well as the structural model of LiPON glass obtained from AIMD [10]. The different ^{31}P local environments were also identified by measuring ^{31}P CSA using two-dimensional (2D) magic-angle turning and phase adjusted sideband separation (MATPASS) [13,14] and by probing ^{31}P - ^{31}P proximities using 1D double-quantum (DQ)-filtered NMR experiments as well as 2D ^{31}P DQ-single-quantum (SQ) through-space homonuclear correlation experiments. Based on these calculations and advanced NMR techniques, the 1D ^{31}P MAS NMR spectrum of LiPON was simulated as the sum of four signals at 19.3, 14.6, 9.3 and 4.7 ppm assigned to PO_3N^{4-} isolated tetrahedra, $[\text{O}_3\text{PNPO}_3]^{5-}$ dimers, PO_4^{3-} orthophosphate and $[\text{O}_3\text{POPO}_3]^{4-}$ pyrophosphate anions, respectively (see Fig. 1). The local environment of ^{31}P nuclei in these species were denoted Q_1^0 , Q_1^1 , Q_0^0 and Q_0^1 , respectively, using Q_m^n nomenclature, where m and n denote the numbers of nitrogen and bridging atoms bound to P atom, respectively.

Nevertheless, this above assignment strongly relies on the structural model obtained by AIMD. Furthermore, the nature of P local environments can depend on the chemical composition of the LiPON thin film and its preparation. Therefore, there is a need for further experimental

evidences to substantiate the proposed assignment.

We report herein new insights into interatomic proximities in LiPON thin films obtained using solid-state NMR spectroscopy. We notably identified ^{31}P sites bound to ^{14}N isotope by measuring the dephasing of ^{31}P signals under ^{31}P - ^{14}N dipolar couplings using transfer of population in double resonance (TRAPDOR) technique [15–17]. Furthermore, the strength of ^{31}P - ^{31}P effective dipolar couplings for the different ^{31}P nuclei was estimated using 1D DQ-filtered spectra as well as dipolar dephasing experiments using DQ-DRENAR (DQ-based dipolar-recoupling effects nuclear alignment reduction) method [18–20]. This novel NMR data about P-N and P-P proximities in LiPON thin films substantiate the recently proposed assignment of ^{31}P NMR spectra [10].

2. Experimental section

2.1. Thin film preparation

LiPON thin films were deposited by rf magnetron sputtering from a γ - Li_3PO_4 target in a chamber (PLASSY MP 300 T) connected to a glove box under an argon atmosphere. The γ - Li_3PO_4 powder was prepared at first by annealing the β - Li_3PO_4 powder (Sigma Aldrich, 99.9%) at 650 °C for 12 h under an argon stream. The target with a diameter of 50 mm was then prepared by spark plasma sintering (SPS) of the γ - Li_3PO_4 powder at 700 °C and 125 kPa in a graphite die. Before thin film depositions, the chamber was evacuated until the pressure was less than 5×10^{-5} Pa and then systematically pre-sputtered for at least 30 min. The films were deposited at a nominal rf power density of 2 W.cm $^{-2}$ and a target-to-substrate distance of 8 cm. LiPON thin films were deposited under a pure nitrogen atmosphere with a flow rate of 40 mL.min $^{-1}$. Deposition rate of about 0.15 $\mu\text{m.h}^{-1}$ was estimated by measuring the thickness of the films using a stylus profilometer (Tencor Alpha-Step 200). Different substrates were employed for film deposition depending on the envisaged characterization. All samples were handled in an argon-filled glove box and transferred to the different apparatuses used for characterization using airtight containers.

2.2. Chemical analysis

The P, N and O contents were determined by means of electron probe micro-analysis (EPMA) employing a CAMECA SX100 equipment. For EPMA, samples were produced by sputtering thin films of about 1 μm on Si_3N_4 substrate previously covered with a gold coating. The thin films were covered with a 20 nm thick gold layer and analyzed by applying a 10 kV excitation voltage. InP, Si_3N_4 and $\text{Y}_3\text{Fe}_5\text{O}_{12}$ compounds were used as calibration standards. Li and P contents were determined using an inductively coupled plasma-optical emission spectrometer (ICP-OES) using a Varian 720ES equipment. Emission line wavelengths of 610.365 nm and 214.914 nm were respectively chosen for Li and P elements. The results of EPMA and ICP-OES were combined to determine the complete elemental composition of the films.

2.3. Solid-state NMR

2.3.1. Sample preparation

LiPON thin films for NMR characterization were deposited on 100 mm diameter silicon wafers, which were previously coated with a polyvinylidene difluoride (PVDF) film to facilitate sample recovery. The PVDF films were prepared on the silicon substrate by spin-coating of a PVDF solution obtained by dissolving 20 g of PVDF in 80 g of N-methyl-2-pyrrolidone. Then 4 mL of the polymer solution were spin coated on the substrate using a Specialty Coating Systems G3 spin coater at a rotation speed of 4000 rpm for 45 s. After coating, the films were dried on a hot plate at 150 °C for 60 s resulting in PVDF films of a few microns. LiPON thin film was then prepared by sputtering to reach a thickness of about 2.5 μm . The samples were collected by scratching the surface of the substrate with a scalpel blade in a glovebox. About 1 mg of the

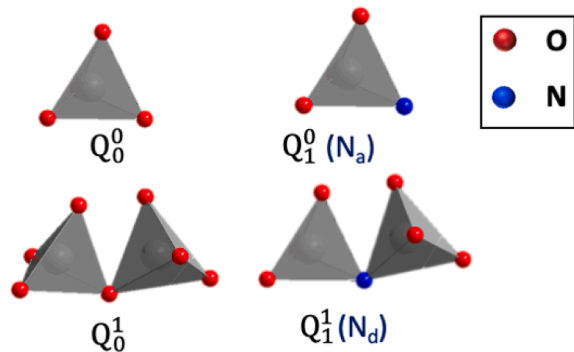


Fig. 1. Four local structural units identified in LiPON thin films in reference [10] using AIMD simulations and ^{31}P solid-state NMR spectroscopy. The P local environment is denoted using Q_m^n nomenclature. The Q_1^0 and Q_1^1 units contain N atoms in the form of N_a and N_d sites, respectively.

resulting powder containing both PVDF and LiPON film was collected and then introduced in a 2.5 mm rotor using silicone inserts to center the sample in the middle of the detection coil (see Fig. S1).

2.3.2. NMR experiments

The NMR experiments were conducted at a static magnetic field $B_0 = 9.4$ T on a Bruker BioSpin Avance NEO NMR spectrometer equipped with a 2.5 mm triple-resonance HXY probe. These experiments used $\pi/2$ and π pulses lasting 2.05 and 4.10 μs , respectively, on ^{31}P channel. Quantitative 1D ^{31}P NMR spectra under MAS conditions were acquired using Bloch-decay experiment at a MAS frequency $\nu_R = 25$ kHz and resulted from averaging 256 transients with a recovery delay, τ_{RD} , equal to 70 s, five times the longest longitudinal relaxation time, T_1 , of ^{31}P nuclei to ensure quantitative NMR measurements. Hence, the total experimental time to acquire this spectrum was 5 h. The ^{31}P T_1 times were estimated using a saturation-recovery sequence involving a burst of presaturation pulses ($20 \pi/2$ pulses separated by 2 ms) followed by a recovery delay ranging from 2 to 128 s. Four transients were acquired for each recovery delay.

Through-space proximities between ^{31}P nuclei were probed using 1D DQ-filtered and 2D DQ-SQ homonuclear correlation experiments, in which ^{31}P homonuclear dipolar couplings were reintroduced under MAS conditions with $\nu_R = 25$ kHz using back-to-back (BaBa-xy16) recoupling schemes of equal length, $12\tau_R = 12/(\nu_R) = 480 \mu\text{s}$, for the excitation and the reconversion of DQ coherences [21]. The 2D ^{31}P BaBa DQ-SQ spectrum resulted from averaging 64 transients for each of 64 t_1 increments with $\Delta t_1 = \tau_R = 40 \mu\text{s}$ and $\tau_{RD} = 20 \text{ s} \approx 1.3 T_1$ to maximize the sensitivity [22]. The total experimental time to acquire this 2D spectrum was 48 h. The 1D ^{31}P BaBa DQ-filtered spectrum resulted from averaging 1024 transients with $\tau_{RD} = 20$ s, leading to a total experimental time of 5 h 40 min.

The strengths of ^{31}P - ^{31}P dipolar couplings were also estimated using DQ-DRENAR experiment [18–20], which is displayed in Fig. S2 and employs POST-C7 recoupling [23] to reintroduce the ^{31}P homonuclear dipolar couplings under MAS conditions with $\nu_R = 10$ and 12.5 kHz. The MAS frequency was lower than for other NMR experiments since the POST-C7 recoupling requires an rf field strength equal to $7\nu_R$ and the rf power specification of the probe prevents its use at $\nu_R = 25$ kHz. For each recoupling time, we recorded both the dephased (S) and reference (S_0) signals and calculated the signal fraction $(S_0 - S)/S_0$. In the reference experiment, the consecutive POST-C7 blocks are shifted by 90° to refocus the evolution under ^{31}P homonuclear dipolar coupling. The recoupling time, $\tau = 4n\tau_R$, with $2n$ the number of POST-C7 blocks, was varied from 320 to 800 μs . Both S and S_0 spectra resulted from averaging 256 transients for each recoupling time with $\tau_{RD} = 20$ s, leading to a total experimental time of 23 h.

The proximities between P and N nuclei were probed using $^{31}\text{P}\{^{14}\text{N}\}$ TRAPDOR experiment with ^{31}P detection (see Fig. S3), in which the ^{31}P - ^{14}N dipolar interactions are reintroduced by continuous wave (CW) irradiation on ^{14}N channel lasting 1.5 ms and employing an rf field strength of 100 kHz during the first half of the spin echo applied to ^{31}P nuclei. We employed TRAPDOR experiment, instead of Rotational-Echo Adiabatic-Passage DOuble-Resonance (REAPDOR) [24] and Resonance-Echo Saturation-Pulse DOuble-Resonance (RESPDOR) [25,26] variants, since in these latter experiments, the heteronuclear dipolar recoupling sequence is applied to the detected isotope, ^{31}P , and reintroduces the ^{31}P CSA, besides the ^{31}P - ^{14}N dipolar interactions. As the employed heteronuclear dipolar recoupling is non- γ -encoded, the refocusing of the ^{31}P CSA requires a perfect synchronization with MAS of the defocusing and refocusing delays. This synchronization is difficult to achieve for the long defocusing and refocusing delays and random fluctuations of the MAS frequency results in imperfect refocusing of the ^{31}P CSA, and hence, variation in signal amplitude from scan to scan [27]. This experiment was performed at $\nu_R = 20$ kHz. We recorded both the dephased (S) and reference (S_0) signals for this TRAPDOR experiment by averaging 5680 transients for each recoupling time with $\tau_{RD} = 20$ s,

leading to a total experimental time of 63 h.

The $\delta_{\text{iso}}(^{31}\text{P})$ shifts were referenced to 85 wt% H_3PO_4 aqueous solution. 1D ^{31}P MAS NMR spectra were simulated using dmfit software [28] as the sum of Gaussian lineshapes since the distribution of ^{31}P local environments results in a distribution of $\delta_{\text{iso}}(^{31}\text{P})$ values.

3. Results and discussion

The chemical composition of the sputtered LiPON thin film was estimated to be $\text{Li}_{3.2}\text{PO}_{3.0}\text{N}_{0.7}$, based on a Li/P ratio of 3.2 determined by ICP-OES and O/P and N/P ratios of 3.0 and 0.7 obtained using EPMA. This latter ratio is significantly higher than those for which structural models have been proposed based on AIMD simulations [8–10]. Nevertheless, the (O+N)/P ratio of 3.7 ranges between that of Li_3PO_4 orthophosphate (O/P ratio = 4) and $\text{Li}_4\text{P}_2\text{O}_7$ pyrophosphate (O/P ratio = 3.5) compounds, indicating a partial dimerization of the initial orthophosphate structure upon nitrogen incorporation.

In spite of the limited amount of sample (less than 1 mg of LiPON thin film in the rotor), we were able to acquire the 1D ^{31}P MAS NMR spectrum of the thin film with a good signal-to-noise ratio in 5 h, as shown in Fig. 2, since this spin-1/2 isotope has favorable NMR properties, including a high gyromagnetic ratio, $\gamma(^{31}\text{P}) = 0.40\gamma(^1\text{H})$, and a 100% natural abundance. This spectrum, which exhibits a broad peak with a maximal intensity at 9 ppm, is slightly broader than that recently reported for LiPON thin films deposited by rf sputtering [10]. The broadening of the peak stems from the distribution of P local environments in LiPON amorphous thin film and the increased broadening might stem from the higher amount of N atoms.

To identify the NMR signals of ^{31}P nuclei close to N atoms, we recorded $^{31}\text{P}\{^{14}\text{N}\}$ TRAPDOR spectra since nitrogen-14, which has a natural abundance of 99.64%, is the most abundant isotope of nitrogen element. As the spectrum of this spin-1/2 nucleus is broadened by quadrupolar interaction in solids, ^{31}P - ^{14}N dipolar interactions were measured using TRAPDOR sequence, which as explained above, is more robust to ^{31}P CSA and MAS instabilities than the REAPDOR and RESPDOR experiments. As the low gyromagnetic ratio of ^{14}N nuclei, $\gamma(^{14}\text{N}) \approx 0.072\gamma(^1\text{H})$, limits the strength of ^{31}P - ^{14}N dipolar interactions, the experiment was performed with a long recoupling time of 1.5 ms resulting in long echo delays and hence, significant signal loss. To the best of our knowledge, $^{31}\text{P}\{^{14}\text{N}\}$ TRAPDOR experiment has not been reported in the literature so far. As seen in Fig. 3, the dephased TRAPDOR spectrum, S ,

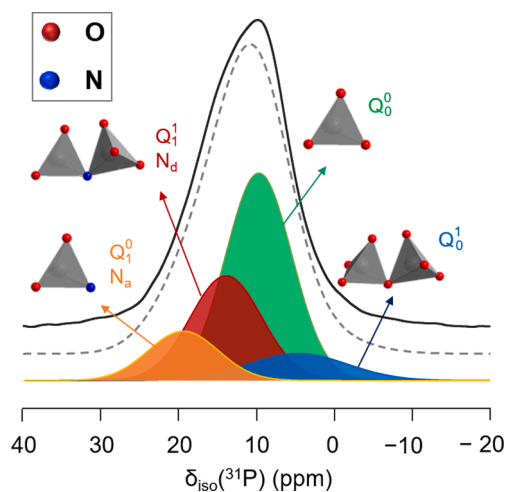


Fig. 2. Experimental (black solid line) and simulated (grey dashed line) quantitative 1D ^{31}P MAS NMR spectrum of LiPON thin film acquired at 9.4 T with $\nu_R = 25$ kHz. The spectrum of LiPON thin films was simulated as the sum of four distinct signals assigned to Q_1^0 , Q_1^1 , Q_0^0 and Q_0^1 P sites by order of decreasing isotropic chemical shift. This deconvolution is based on the NMR data reported in this article as well as the assignment proposed in ref. [10].

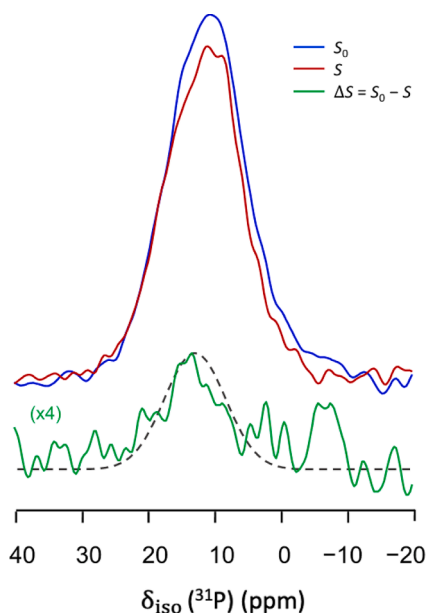


Fig. 3. Experimental S (red solid line) and S_0 (blue solid line) $^{31}\text{P}\{^{14}\text{N}\}$ TRAPDOR spectra of LiPON thin film acquired at 9.4 T with $\nu_R = 20$ kHz. Experimental (green solid line) and simulated (grey dashed line) difference spectra $\Delta S = S_0 - S$ are also displayed with intensities multiplied by a factor of 4 with respect to S and S_0 spectra.

exhibits reduced intensity with respect to the reference spectrum, S_0 , for $\delta_{\text{iso}}(^{31}\text{P}) \approx 13\text{--}14$ ppm, yielding a peak with a maximum at this shift in the difference spectrum, $\Delta S = S_0 - S$. This peak can be roughly simulated as a Gaussian line with $\delta_{\text{iso}}(^{31}\text{P}) \approx 13.6$ ppm and a full-width at half maximum (FWHM) of 10.8 ppm. Hence, the ^{31}P nuclei with $\delta_{\text{iso}}(^{31}\text{P}) \approx 13.6$ ppm are closer to ^{14}N isotope than those with lower isotropic chemical shift. This result substantiates that NMR signal near 14 ppm must be assigned to ^{31}P nuclei bound to N atom, whereas that near 9 ppm stems from those only surrounded by O atoms. Nevertheless, the signal-to-noise ratio of TRAPDOR spectra are too low to conclude about the proximities with nitrogen atoms for ^{31}P nuclei with $\delta_{\text{iso}}(^{31}\text{P}) \approx 19$ and 5 ppm.

The $^{31}\text{P}\text{-}^{31}\text{P}$ proximities were probed by recording 1D DQ-filtered spectrum for ^{31}P isotope. As seen in Fig. 4, the 1D DQ-filtered spectrum compared to the MAS spectrum displays a lower relative intensity at $\delta_{\text{iso}}(^{31}\text{P}) \approx 8$ ppm with respect to that at $\delta_{\text{iso}}(^{31}\text{P}) \approx 14$ ppm and the difference between these spectra exhibits a peak near 8 ppm. The position of this peak only weakly depends on the baseline and phase

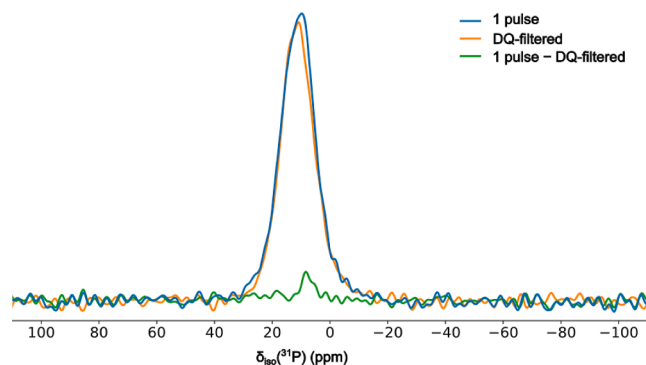


Fig. 4. Experimental 1D ^{31}P MAS (blue) and DQ-filtered (orange) NMR spectra of LiPON thin film acquired at 9.4 T with $\nu_R = 25$ kHz. The experimental (green) difference spectrum is also displayed. It was obtained by subtracting the 1D DQ-filtered spectrum to its 1D MAS counterpart after equalizing their intensities at 13 ppm.

corrections (see Fig. S4). Hence, the ^{31}P nuclei resonating at 8 ppm exhibit lower effective $^{31}\text{P}\text{-}^{31}\text{P}$ dipolar couplings than those near 14 ppm. Therefore, the line resonating at 13.6 ppm corresponds to ^{31}P nuclei close to N atom and another ^{31}P nucleus, whereas that near 8 ppm is produced by P sites more distant from N and P atoms.

The $^{31}\text{P}\text{-}^{31}\text{P}$ proximities were further investigated by recording 2D ^{31}P through-space DQ-SQ homonuclear correlation spectrum, as seen in Fig. 5. This spectrum is dominated by an autocorrelation peak with a maximum near $\delta_{\text{iso}} \approx 14$ ppm, which suggests that the corresponding ^{31}P nuclei are bound together. As this peak has a width of about 10 ppm, it also produces lower nonzero intensity along the diagonal near 19 and 9 ppm and masks possible autocorrelation peaks at these shifts. Conversely, this autocorrelation peak centered at 14 ppm cannot explain the nonzero intensity near the diagonal for δ_{iso} values ranging from 0 to 5 ppm. Therefore, the LiPON thin film must contain a third ^{31}P local environment with $\delta_{\text{iso}} \approx 5$ ppm bound to similar site. Furthermore, the absence of off-diagonal peaks in this 2D spectrum indicates that the distinct P local environments are more distant than the covalently bound identical P sites and hence, the LiPON thin films do not contain covalent bonds between the distinct P sites.

Based on the previous experimental results, we first tried to simulate the 1D ^{31}P MAS spectrum shown in Fig. 2 as the sum of three Gaussian lines using as initial δ_{iso} values, 13.6, 8 and 5 ppm, and FWHM ≈ 10 ppm. Nevertheless, no correct simulated spectrum could be obtained in that case. Conversely the experimental spectrum could be properly simulated when considering an additional Gaussian line with $\delta_{\text{iso}} = 19.4$ ppm, as seen in Fig. 2. The best-fit simulation parameters are given in Table 1. The signal at 13.9 ppm, produced by ^{31}P nuclei close to N atoms and to ^{31}P nuclei with similar isotropic chemical shifts, can be assigned to dimers of Q_1^1 sites in agreement with the structural model derived by AIMD simulation [10], whereas the signal at 9.7 ppm, which corresponds to ^{31}P nuclei surrounded by O atoms and more distant from other ^{31}P nuclei, must stem from Q_0^0 site of orthophosphate anions. The best-fit δ_{iso} and FWHM parameters of Q_1^1 and Q_0^0 sites slightly differ from those determined from $^{31}\text{P}\{^{14}\text{N}\}$ TRAPDOR and ^{31}P DQ-filtered spectra. The signals at 19.4 and 4.7 ppm were assigned to Q_1^0 and Q_0^1 local environments based the assignment recently derived using AIMD simulations and DFT calculation of NMR parameters [10]. This assignment is consistent with the observation of an autocorrelation peak near 5 ppm in

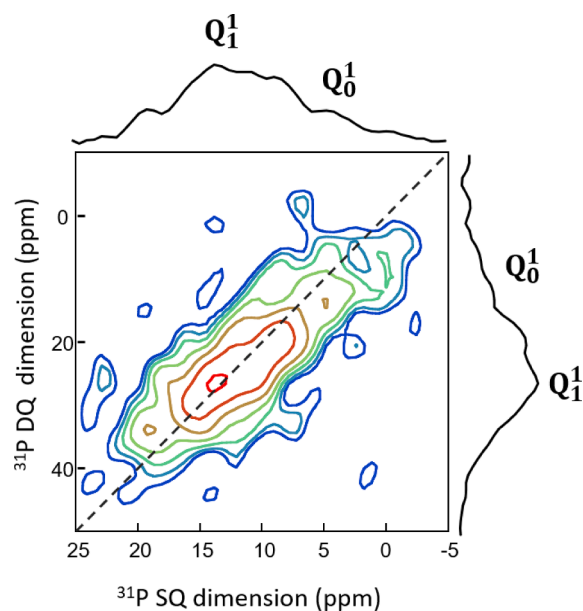


Fig. 5. 2D ^{31}P through-space DQ-SQ homonuclear correlation spectrum of LiPON thin film acquired at 9.4 T with $\nu_R = 25$ kHz along with its sum projections along both dimensions.

Table 1

Parameters used to simulate the quantitative 1D ^{31}P MAS NMR spectrum of LiPON thin film. Error bars are indicated.

Site	Q_1^0	Q_1^1	Q_0^0	Q_0^1
$\delta_{\text{iso}}(^{31}\text{P})$ (ppm)	19.4 ± 0.3	13.9 ± 0.2	9.7 ± 0.1	4.7 ± 0.3
FWHM (ppm)	10.6 ± 0.4	10.8 ± 0.3	10.0 ± 0.2	15.0 ± 0.4
Fraction (%)	12.6 ± 0.4	27.3 ± 0.2	50.1 ± 0.2	9.9 ± 0.3

Fig. 5. Hence, this NMR study confirms that the LiPON thin film contains four main distinct P local environments, Q_1^0 , Q_1^1 , Q_0^0 and Q_0^1 , by decreasing order of δ_{iso} . Half of the P atoms occupy Q_0^0 sites, whereas the molar fraction of other environments decreases in the following order: $Q_1^1 > Q_1^0 > Q_0^1$. The measured δ_{iso} shifts for the four sites are comparable to those previously reported [10]. Conversely the FWHM of the four signals are significantly larger. Furthermore, the amount of Q_1^1 sites is slightly reduced, whereas the fraction of Q_0^0 environments is slightly enhanced. These differences might stem from variations in the chemical composition, such as higher amount of N element, and sample preparation conditions between the two LiPON thin films

The proximities between ^{31}P nuclei were also quantified by recording DQ-DRENAR experiment. For the different recoupling times, τ , the reference and dephased DQ-DRENAR spectra, S_0 and S , were simulated (see Fig. S5) using δ_{iso} and FWHM values given in Table 1 to calculate the signal fraction, $(S_0 - S)/S_0$ for the four distinct sites (see Fig. 6). The effective ^{31}P homonuclear dipolar coupling constant, $b_{\text{pp}}^{\text{eff}}/(2\pi)$, in Hz for each site j was estimated by fitting the signal fraction to the parabolic equation below for short recoupling time:

$$\frac{S_0 - S}{S_0} = 0.56 \left(\frac{b_{\text{pp}}^{\text{eff}}}{2\pi} \tau \right)^2 \quad (1)$$

where

$$\frac{b_{\text{pp}}^{\text{eff}}}{2\pi} = \sqrt{\sum_k \left(\frac{b_{jk}}{2\pi} \right)^2} \quad (2)$$

where k denotes all spins coupled to the spin j and $b_{jk}/(2\pi)$ the dipolar coupling constant in Hz between the spins j and k . The signal-to-noise ratios for Q_1^0 and Q_0^1 sites were too low to estimate a correct effective homonuclear dipolar coupling constant. Conversely, we measured using Eq. (1) $b_{\text{pp}}^{\text{eff}}/(2\pi)$ constants equal to 1118 and 975 Hz for Q_1^1 and Q_0^0 , respectively. These values confirm the closer proximities between P atoms for signal resonating at 13.9 ppm and hence, its assignment to Q_1^1 sites of dimeric anions.

4. Conclusion

Despite the limited volume of amorphous LiPON thin films prepared by rf sputtering and their sensitivity to air, we demonstrated that advanced solid-state NMR experiments, including $^{31}\text{P}\{^{14}\text{N}\}$ TRAPDOR and ^{31}P DQ-DRENAR, can provide new insights into ^{31}P , ^{14}N and ^{31}P - ^{31}P proximities in these solid electrolytes employed in most commercial microbatteries. These novel NMR data indicate the presence of four distinct ^{31}P sites in LiPON thin films. Their isotropic chemical shift and internuclear proximities are consistent with the assignment recently proposed on the basis of AIMD simulations and DFT calculations of NMR parameters. The quantitative ^{31}P NMR measurements show that the most abundant species are PO_4^{3-} orthophosphate anions, followed $[\text{O}_3\text{PNPO}_3]^{5-}$ dimers, but PO_3N^{4-} isolated tetrahedra and $[\text{O}_3\text{POPO}_3]^{4-}$ pyrophosphate anions are also present, which is in agreement with a P/(O + N) ratio comprised between 3.5 and 4. The possibility to probe the atomic-level structure of LiPON thin films using ^{31}P solid-state NMR spectroscopy opens new avenues to understand the relationships

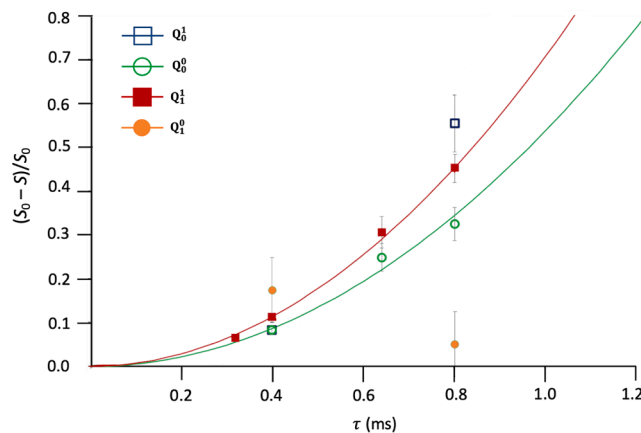


Fig. 6. Experimental ^{31}P DQ-DRENAR signal fraction as function of recoupling time, τ , for Q_1^1 (orange solid disk), Q_1^0 (red solid square), Q_0^0 (green open circle) and Q_0^1 (blue open square) sites of LiPON thin film acquired at 9.4 T and $\nu_R = 10$ kHz (for $\tau = 0.40$ and 0.80 ms) and 12.5 kHz (for $\tau = 0.32$ and 0.64 ms) along the best-fit parabola to estimate the effective ^{31}P homonuclear dipolar coupling constants for the Q_1^1 and Q_0^0 sites. The error bars were determined from the deconvolution of 1D S_0 and S DQ-DRENAR spectra shown in Fig. S5.

between the chemical compositions and the ionic conductivity of these solid electrolytes.

Declaration of Competing Interest

The authors declare the following financial interests/personal relationships which may be considered as potential competing interests: [Olivier Lafon reports financial support was provided by French National Research Agency.].

Data availability

Data will be made available on request.

Acknowledgements

Chevreur Institute (FR 2638), Ministère de l'Enseignement Supérieur et de la Recherche, Hauts-de-France Region, and FEDER are acknowledged for supporting and funding partially this work. Financial support from the IR INFRANALYTICS FR2054 CNRS for conducting the research is gratefully acknowledged. The authors also acknowledge financial support of contract ANR-18-CE08-0015-01 (ThinGlass).

Appendix A. Supplementary material

Supplementary data to this article can be found online at <https://doi.org/10.1016/j.jmr.2023.107530>.

References

- [1] Q. Xia, F. Zan, Q. Zhang, W. Liu, Q. Li, Y. He, J. Hua, J. Liu, J. Xu, J. Wang, C. Wu, H. Xia, All-Solid-State thin film lithium/lithium-ion microbatteries for powering the Internet of Things, *Adv. Mater.* 35 (2023) 2200538, <https://doi.org/10.1002/adma.202200538>.
- [2] Z. Zhu, R. Kan, S. Hu, L. He, X. Hong, H. Tang, W. Luo, Recent advances in high-performance microbatteries: construction, application, and perspective, *Small* 16 (2020) 2003251, <https://doi.org/10.1002/sml.202003251>.
- [3] J. Bates, Electrical properties of amorphous lithium electrolyte thin films, *Solid State Ion.* 53–56 (1992) 647–654, [https://doi.org/10.1016/0167-2738\(92\)90442-R](https://doi.org/10.1016/0167-2738(92)90442-R).
- [4] C.S. Nimisha, K.Y. Rao, G. Venkatesh, G.M. Rao, N. Munichandraiah, Sputter deposited LiPON thin films from powder target as electrolyte for thin film battery applications, *Thin Solid Films.* 519 (2011) 3401–3406, <https://doi.org/10.1016/j.tsf.2011.01.087>.

- [5] B. Fleutot, B. Pecquenard, H. Martinez, M. Letellier, A. Levasseur, Investigation of the local structure of LiPON thin films to better understand the role of nitrogen on their performance, *Solid State Ion.* 186 (2011) 29–36, <https://doi.org/10.1016/j.ssi.2011.01.006>.
- [6] Y. Su, J. Falgenhauer, A. Polity, T. Leichtweiß, A. Kronenberger, J. Obel, S. Zhou, D. Schlettwein, J. Janek, B.K. Meyer, LiPON thin films with high nitrogen content for application in lithium batteries and electrochromic devices prepared by RF magnetron sputtering, *Solid State Ion.* 282 (2015) 63–69, <https://doi.org/10.1016/j.ssi.2015.09.022>.
- [7] F. Muñoz, Comments on the structure of LiPON thin-film solid electrolytes, *J. Power Sources* 198 (2012) 432–433, <https://doi.org/10.1016/j.jpowsour.2011.09.009>.
- [8] V. Lacivita, A.S. Westover, A. Kercher, N.D. Phillip, G. Yang, G. Veith, G. Ceder, N. J. Dudney, Resolving the amorphous structure of lithium Phosphorus Oxynitride (LiPON), *J. Am. Chem. Soc.* 140 (2018) 11029–11038, <https://doi.org/10.1021/jacs.8b05192>.
- [9] V. Lacivita, N. Artrith, G. Ceder, Structural and compositional factors that control the Li-Ion conductivity in LiPON electrolytes, *Chem. Mater.* 30 (2018) 7077–7090, <https://doi.org/10.1021/acs.chemmater.8b02812>.
- [10] M.A.T. Marple, T.A. Wynn, D. Cheng, R. Shimizu, H.E. Mason, Y.S. Meng, Local Structure of Glassy Lithium Phosphorus Oxynitride Thin Films: A Combined Experimental and Ab Initio Approach, *Angew. Chem. Int. Ed.* 59 (2020) 22185–22193, <https://doi.org/10.1002/anie.202009501>.
- [11] N. Mascaraque, A. Durán, F. Muñoz, G. Tricot, Structural features of LiPON glasses determined by 1D and 2D ^{31}P MAS NMR, *Int. J. Appl. Glass Sci.* 7 (2016) 69–79, <https://doi.org/10.1111/ijag.12120>.
- [12] P.E. Stallworth, F. Vereda, S.G. Greenbaum, T.E. Haas, P. Zerigian, R.B. Goldner, Solid-State NMR studies of lithium phosphorus oxynitride films prepared by nitrogen ion beam-assisted deposition, *J. Electrochem. Soc.* 152 (2005) A516–A522, <https://doi.org/10.1149/1.1856922>.
- [13] I. Hung, L. Zhou, F. Pourpoint, C.P. Grey, Z. Gan, Isotropic high field NMR spectra of Li-ion battery materials with anisotropy >1 MHz, *J. Am. Chem. Soc.* 134 (2012) 1898–1901, <https://doi.org/10.1021/ja209600m>.
- [14] I. Hung, T. Edwards, S. Sen, Z. Gan, MATPASS/CPMG: a sensitivity enhanced magic-angle spinning sideband separation experiment for disordered solids, *J. Magn. Reson.* 221 (2012) 103–109, <https://doi.org/10.1016/j.jmr.2012.05.013>.
- [15] C.P. Grey, W.S. Veeman, The detection of weak heteronuclear coupling between spin 1 and spin 1/2 nuclei in MAS NMR; $^{14}\text{N}/^{13}\text{C}/^1\text{H}$ triple resonance experiments, *Chem. Phys. Lett.* 192 (1992) 379–385, [https://doi.org/10.1016/0009-2614\(92\)85486-T](https://doi.org/10.1016/0009-2614(92)85486-T).
- [16] C.P. Grey, W.S. Veeman, A.J. Vega, Rotational echo $^{14}\text{N}/^{13}\text{C}/^1\text{H}$ triple resonance solid-state nuclear magnetic resonance: a probe of $^{13}\text{C}-^{14}\text{N}$ internuclear distances, *J. Chem. Phys.* 98 (1993) 7711–7724, <https://doi.org/10.1063/1.464579>.
- [17] C.P. Grey, A.J. Vega, Determination of the Quadrupole Coupling Constant of the Invisible Aluminum Spins in Zeolite HY with $^1\text{H}-^{27}\text{Al}$ TRAPDOR NMR, *J. Am. Chem. Soc.* 117 (1995) 8232–8242, <https://doi.org/10.1021/ja00136a022>.
- [18] J. Ren, H. Eckert, A homonuclear rotational echo double-resonance method for measuring site-resolved distance distributions in $I=1/2$ spin pairs, clusters, and multispin systems, *Angew. Chem. Int. Ed.* 51 (2012) 12888–12891, <https://doi.org/10.1002/anie.201207094>.
- [19] J. Ren, H. Eckert, DQ-DRENAR: A new NMR technique to measure site-resolved magnetic dipole-dipole interactions in multispin-1/2 systems: theory and validation on crystalline phosphates, *J. Chem. Phys.* 138 (2013), 164201, <https://doi.org/10.1063/1.4801634>.
- [20] J. Ren, H. Eckert, Applications of DQ-DRENAR for the structural analysis of phosphate glasses, *Solid State Nucl. Magn. Reson.* 72 (2015) 140–147, <https://doi.org/10.1016/j.ssnmr.2015.10.009>.
- [21] K. Saalwächter, F. Lange, K. Matyjaszewski, C.-F. Huang, R. Graf, BaBa-xy16: robust and broadband homonuclear DQ recoupling for applications in rigid and soft solids up to the highest MAS frequencies, *J. Magn. Reson.* 1997 212 (2011) 204–215, <https://doi.org/10.1016/j.jmr.2011.07.001>.
- [22] M. Pons, M. Feliz, E. Giralt, Steady-State DQF-COSY Spectra Using a Variable Relaxation Delay, *J. Magn. Reson.* 78 (1988) 314–320.
- [23] M. Hohwy, H.J. Jakobsen, M. Edén, M.H. Levitt, N.C. Nielsen, Broadband dipolar recoupling in the nuclear magnetic resonance of rotating solids: a compensated C7 pulse sequence, *J. Chem. Phys.* 108 (1998) 2686–2694.
- [24] T. Gullion, Measurement of dipolar interactions between spin-1/2 and quadrupolar nuclei by rotational-echo, adiabatic-passage, double-resonance NMR, *Chem. Phys. Lett.* 246 (1995) 325–330.
- [25] Z. Gan, Measuring multiple carbon-nitrogen distances in natural abundant solids using R-RESPDOR NMR, *Chem. Commun.* (2006) 4712–4714, <https://doi.org/10.1039/b611447d>.
- [26] L. Chen, Q. Wang, B. Hu, O. Lafon, J. Trébosc, F. Deng, J.-P. Amoureux, Measurement of hetero-nuclear distances using a symmetry-based pulse sequence in solid-state NMR, *Phys. Chem. Chem. Phys.* 12 (2010) 9395–9405, <https://doi.org/10.1039/b926546e>.
- [27] A. Venkatesh, X. Luan, F.A. Perras, I. Hung, W. Huang, A.J. Rossini, t_1 -Noise eliminated dipolar heteronuclear multiple-quantum coherence solid-state NMR spectroscopy, *Phys. Chem. Chem. Phys.* 22 (2020) 20815–20828, <https://doi.org/10.1039/D0CP03511D>.
- [28] D. Massiot, F. Fayon, M. Capron, I. King, S. Le Calvé, B. Alonso, J.-O. Durand, B. Bujoli, Z. Gan, G. Hoatson, Modelling one- and two-dimensional solid-state NMR spectra: Modelling 1D and 2D solid-state NMR spectra, *Magn. Reson. Chem.* 40 (2002) 70–76, <https://doi.org/10.1002/mrc.984>.